Proceedings of 12th European Conference on Turbomachinery Fluid dynamics
Paper ID: ETC2017-196 & Thermodynamics ETC12, April 3-7, 2017; Stockholm, Sweden

OPTIMAL PERTURBATIONS IN TRANSITIONAL AND TURBULENT FLOWS AT MODERATE REYNOLDS NUMBERS

M. Farano[1,2]*, S. Cherubini*[1]*, J. C. Robinet*[2] *and P. De Palma*[1]

[1]DMMM, Politecnico di Bari, Via Re David 200, 70125 Bari, Italy
[2]DynFluid Laboratory, Arts et Metiers ParisTech, 151 Boulevard de l'Hopital, 75013 Paris, France

ABSTRACT

The development of accurate transition and turbulence models is of fundamental interest for predicting flows in turbomachinery and improving their design. Recently developed optimization techniques, based on Lagrangian multipliers approach and direct-adjoint iterations, allow one to investigate the basic mechanisms by which perturbations grow and turbulence is self-sustained in wall-bounded flows. In particular, employing the linearized Navier–Stokes equations, the lift-up effect has been found to be responsible of the transient growth of the perturbations and of the by-pass transition. In the present work, the extension of the optimization approach to the nonlinear equations is described, both for the cases of transitional and turbulent flows. Optimal coherent structures are identified, such as large scale streaks and hairpin vortices, which carry a great part of the Reynolds stresses. Such coherent structures are a suitable starting point for the development of reduced-order models of turbulence.

INTRODUCTION

Turbulence is a widespread complex phenomenon influencing, in particular, the performance of turbomachinery. In fact, in turbomachinery flows, boundary-layer transition from laminar to turbulent flow and the structure of the turbulent boundary layer remarkably affect the friction coefficient at wall, the flow separation (stall), and the heat transfer. Yet, achieving a thorough comprehension of the dynamics of wall-bounded turbulent flow remains a formidable challenge since turbulence appears in a variety of different states and patterns competing with the ordered laminar state (Barkley *et al.*, 2015).

Due to the complexity of such phenomena, the development of accurate low-order models is a suitable route for improving the design process of tubomachinery. To determine low-order models for the onset of chaotic motion from a laminar regime, recent studies have turned the attention to the dynamics of large scale structures, neglecting the random small scale motion: two main examples are the direct percolation model (Lemoult *et al.*, 2016) and the front propagation scenario (Barkley *et al.*, 2015), explaining the coexistence of turbulent patterns competing with the ordered laminar state in the transitional regime.

Even when the flow reaches a fully developed turbulent regime, it remains characterized by small-scale chaotic fluctuations as well as coherent structures, i.e. fluid motions highly correlated over both space and time (Panton, 2001), with characteristic wavelengths and lifetimes. From a dynamical point of view, this coherent motion carries a much larger momentum than the chaotic motion at small scales; thus, a careful characterization of such structures bears an enormous potential for modeling and controlling the self-sustained turbulence dynamics.

First evidence of the existence of exact coherent solutions of the Navier–Stokes equations was given by Nagata (1990) for plane Couette flow and by the vortex-wave interaction theory of Hall & Smith (1991) for high Reynolds numbers. Later, grounding on linear modal and non-modal instability analysis, several authors (Hamilton *et al.*, 1995; Waleffe, 1997) have explained the mechanism driving coherent streaky structures close to the wall in transitional and turbulent flows by a self-sustained process composed of the following three steps: i) streamwise streaks originate from weak streamwise vortices (this process is known as "lift-up" mechanism and generates a transient growth of the perturbation energy); ii) saturating nonlinearly, they become prone to secondary instability; iii) the consequent streak oscillations recreate streamwise vorticity by nonlinear interactions, leading back to the first step. It is noteworthy that flow structures composed by streaks and vortices, similar to those characterizing the first step of the self-sustained mechanism, are involved in a linear transient energy-maximization mechanism as demonstrated by Butler & Farrell (1993).

Other authors (Adrian, 2007; Tomkins & Adrian, 2003) have observed that large-scale coherent structures populate the outer region of wall-bounded turbulent flows, with average spanwise length of O(h) (h being the outer length scale, for instance the half height of a channel flow or the boundary-layer thickness of the flow over a flat plate). These large-scale structures have the form of packets of hairpin vortices (Adrian, 2007; Wu & Moin, 2009) or large-scale oscillating streaks (Tomkins & Adrian, 2003). The presence of packets of hairpin vortices has been also predicted in pipe flow by the theory of Sharma & McKeon (2013) using a superposition of response modes taking the form of traveling waves. Seyadi *et al.* (2013) show that, for the case of boundary-layer flow, for very different transition scenarios, such as H-type, K-type, or by-pass transition, flow statistics in the final phase of transition collapse and the flow is dominated by packets of hairpin vortices. Moreover, the mean and Reynolds stress profile of this transitional flow are in very close agreement with statistics of developed turbulence. Therefore, the hairpin packets represent a structural basic feature of wall-bounded turbulence, at least in the transitional regime.

The present work aims at investigating whether the formation of hairpin vortical structures in wall-bounded transitional and turbulent flow is governed by an energy maximization process on a suitable time scale. The idea is inspired by the linear transient growth analysis which has been employed to explain the linear growth of streaky structures in turbulent flows (Butler & Farrell, 1993). Here, a nonlinear approach is employed for studying highly energetic transient events characterized by ejections and sweeps, using a Lagrange-multipliers optimization technique coupled with a direct-adjoint iterative procedure (Pringle *et al.*, 2012; Cherubini *et al.*, 2010; Cherubini & De Palma, 2013) for computing optimal perturbations.

PROBLEM FORMULATION

In the present section two formulations of the optimization problem are presented. The first formulation applies to laminar flows whereas the second is designed for turbulent flows. The fundamental difference is in the definition of the "base" flow and of the corresponding "perturbation". For laminar flows, the base flow is the exact steady solution of the Navier–Stokes (NS) equation with given boundary conditions; the perturbation to the laminar flow may evolve in time toward transition to turbulence provided that suitable conditions are satisfied. For turbulent flows, one has to define a non-trivial base flow, which is not an exact solution of the Navier–Stokes equations, but usually a mean flow; moreover, in this case, the perturbation is the sum of coherent and chaotic contributions.

Transitional flow

For transitional flows, the nonlinear optimization procedure is employed looking for perturbations of the laminar base flow which are able to induce the largest perturbation energy growth at a short target time. The general technique developed by the authors (Cherubini *et al.*, 2010) to find global optimal perturbations is here briefly recalled. Using such an approach we are able to prove the existence of a nonlinear amplification mechanism of the disturbances which is more effective with respect to the linear one and capable to lead the flow to turbulence for lower values of the perturbation amplitude. Moreover, we can identify the typical flow structures involved in the optimal evolution towards turbulence.

We look for the velocity perturbation $\mathbf{u}$ at $t = 0$ (initial time), having a given initial energy E_0, which can induce at a target time T the highest perturbation energy $E(T) = \{\mathbf{u}(T) \cdot \mathbf{u}(T)\}$, where the symbol $\{\ \}$ indicates integration over the considered three-dimensional domain. This *optimal* perturbation is computed by means of a Lagrange multiplier optimization, which consists in finding extrema of the augmented functional

$$\begin{aligned}\mathfrak{L} = \frac{E(T)}{E(0)} - \int_0^T \left\{p^\dagger \nabla \cdot \mathbf{u}\right\} dt - \int_0^T \left\{\mathbf{u}^\dagger \cdot \left(\frac{\partial \mathbf{u}}{\partial t}\right.\right. \\ \left.\left. + \mathbf{u} \cdot \nabla \mathbf{U} + \mathbf{U} \cdot \nabla \mathbf{u} + \mathbf{u} \cdot \nabla \mathbf{u} + \nabla p - \frac{\nabla^2 \mathbf{u}}{Re}\right)\right\} dt - \lambda \left(\frac{E_0}{E(0)} - 1\right).\end{aligned} \tag{1}$$

In equation (1), the Navier-Stokes equations (written in perturbative formulation with respect to the exact laminar solution) have been imposed as constraint; $(\mathbf{u}^\dagger, p^\dagger)$ and λ are the Lagrange multipliers, namely, the adjoint variables, and Re is the Reynolds number.

Integrating by parts and setting to zero the first variation of $\mathcal{L}$ with respect to $(\mathbf{u}, p)$ leads to the adjoint equations plus the compatibility condition (not shown for brevity, see Cherubini *et al.* (2010) for details).

The optimization procedure for a chosen target time T can be summarized by the following loop: 1) An initial guess is taken for the initial condition, $\mathbf{u}(0)$, with an associated initial energy E_0. 2) The direct problem is integrated up to $t = T$. 3) The adjoint variables, $\mathbf{u}^\dagger(T)$, are provided by the compatibility condition $2\mathbf{u}(T)/E(0) - \mathbf{u}^\dagger(T) = 0$. 4) The adjoint problem is integrated backward in time from $t = T$ to $t = 0$. 5) At $t = 0$, the initial direct state is updated in the direction of the gradient, where the gradient of $\mathcal{L}$ with respect to $\mathbf{u}(0)$ is $\partial\mathcal{L}/\partial\mathbf{u}(0) = -2\mathbf{u}(0)\left(\{\mathbf{u}(T) \cdot \mathbf{u}(T)\} - \lambda E_0\right) / \left\{\mathbf{u}(0) \cdot \mathbf{u}(0)\right\} + \left\{\mathbf{u}^\dagger(0)\right\}$. 6) The objective function $E(T)$ is evaluated: if its variation between two successive iterations is smaller than the chosen threshold $e = 10^{-6}$ the loop is stopped, otherwise the procedure is restarted from step 2).

Turbulent flow

For turbulent flows, the optimization procedure is applied to the Reynolds-averaged Navier–Stokes equations in order to study the dynamics of finite-amplitude perturbations. We split the flow vector $\mathbf{q} = [\mathbf{u}, p]^T$, composed of the velocity vector and pressure, into a mean flow component $\mathbf{Q} = [U, 0, 0, P]^T$ and a disturbance $\tilde{\mathbf{q}} = [\tilde{u}, \tilde{v}, \tilde{w}, \tilde{p}]^T$. Injecting this decomposition in the NS equations, the following equations for the dynamic of the perturbations are obtained:

$$\frac{\partial \tilde{\mathbf{u}}}{\partial t} + \tilde{\mathbf{u}} \cdot \nabla \tilde{\mathbf{u}} + \mathbf{U} \cdot \nabla \tilde{\mathbf{u}} + \tilde{\mathbf{u}} \cdot \nabla \mathbf{U} = -\nabla \tilde{\mathbf{p}} + \frac{1}{Re} \nabla^2 \tilde{\mathbf{u}} + \nabla \cdot \tau, \qquad \nabla \cdot \tilde{\mathbf{u}} = 0. \tag{2}$$

where $\tau = \overline{\tilde{\mathbf{u}}\tilde{\mathbf{u}}}$ is the the Reynolds stress tensor that needs to be known or modeled for closing the problem. This term appears when the perturbative formulation employs a base flow $\mathbf{U}$

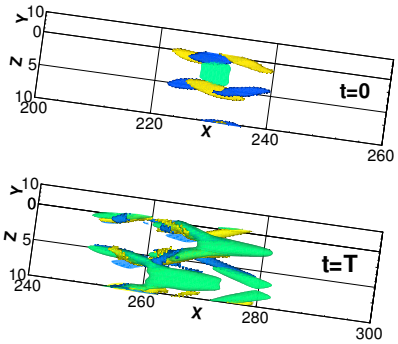

Figure 1: Optimal perturbation: green indicates the streamwise component ($u = -0.01$ at $t = 0$ and $u = -0.1$ at $t = 75$); blue and red indicate negative and positive spanwise components, respectively ($w = \pm 0.007$ at $t = 0$ and $w = \pm 0.05$ at $t = 75$).

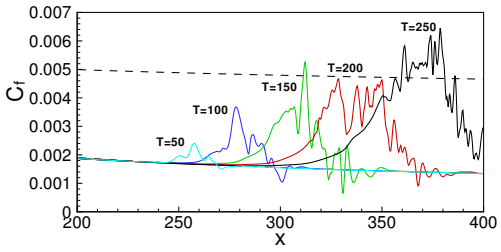

Figure 2: Streamwise distribution of the spanwise-averaged skin-friction coefficient for $T = 50, 100, 150, 200, 250$ (solid lines from left to right) together with the laminar and turbulent theoretical distributions (bottom and top dashed lines, respectively).

which is not a solution of the steady Navier–Stokes equations. Here, we compute τ a-priori by a fully turbulent direct numerical simulation (DNS) in the same flow conditions and $\nabla \cdot \tau$ has the role of a steady forcing, depending only on the wall-normal direction for the channel flow. Using equations (2), we look for perturbations capable of inducing a peak of kinetic energy in a finite time T. Thus, we maximize the kinetic energy growth of the disturbance at time T, $G(T) = E(T)/E(0)$, where $E(t) = \{\tilde{\mathbf{u}}(t) \cdot \tilde{\mathbf{u}}(t)\}$. The energy gain $G(T)$ is maximized using a Lagrange multiplier approach, the initial energy E_0, equations (2), and the incompressibility condition being imposed as constraints using the Lagrange multipliers or adjoint variables $(\widetilde{\mathbf{u}}^\dagger, \widetilde{p}^\dagger)$, as follows:

$$\mathfrak{L} = \frac{E(T)}{E(0)} - \int_0^T \left\{ \widetilde{\mathbf{u}}^\dagger \cdot \widetilde{NS} \right\} dt - \int_0^T \left\{ \widetilde{p}^\dagger \cdot (\nabla \cdot \widetilde{\mathbf{u}}) \right\} dt - \lambda \left(\frac{E(0)}{E_0} - 1 \right), \qquad (3)$$

where $\widetilde{NS}$ represents the Navier–Stokes operator given by equation (2). Deriving the functional $\mathfrak{L}$ with respect to the variables $\tilde{\mathbf{u}}, \tilde{p}$, one obtains the following adjoint equations:

$$\frac{\partial \widetilde{\mathbf{u}}^\dagger}{\partial t} = \widetilde{\mathbf{u}}^\dagger \cdot (\nabla \mathbf{U})^T - \mathbf{U} \cdot \nabla \widetilde{\mathbf{u}}^\dagger - \nabla \mathrm{p}^\dagger - \frac{1}{Re} \Delta \widetilde{\mathbf{u}}^\dagger + \widetilde{\mathbf{u}}^\dagger \cdot (\nabla \widetilde{\mathbf{u}})^T - \widetilde{\mathbf{u}} \cdot \nabla \widetilde{\mathbf{u}}^\dagger, \qquad \nabla \cdot \tilde{\mathbf{u}}^\dagger = 0. \quad (4)$$

Following the optimization loop previously described in the case of transitional flows, (see Pringle *et al.* (2012), Cherubini *et al.* (2010), Duguet *et al.* (2013), Cherubini & De Palma (2013), Cherubini *et al.* (2015)), the optimisation problem is solved by direct-adjoint iterations coupled with a gradient rotation algorithm (Foures *et al.*, 2013; Farano *et al.*, 2016).

RESULTS

Transitional flow

A transitional-flow study is presented concerning a boundary-layer flow. The Reynolds number is defined as $Re = U_\infty \delta^* / \nu$, where ν, δ^*, and U_∞ are the kinematic viscosity, the inflow boundary-layer displacement thickness and the freestream velocity, respectively, and are

employed to nondimensionalise the flow variables. The three-dimensional perturbation vanishes at the bottom and upper-boundary points of the computational box, whereas periodicity is imposed in the spanwise homogeneous direction. Since the flow is not periodic in the streamwise direction, a zero perturbation condition is imposed at inflow and outflow by means of two fringe regions which allow the perturbation to vanish smoothly. The inflow points of the optimization domain are placed at $x_{in} = 200$ with respect to the leading edge of the plate. The direct and adjoint equations are integrated by a second-order-accurate fractional step method using a staggered grid (Verzicco & Orlandi, 1996). A second-order-accurate centered space discretization is used. An optimization domain with dimensions $L_x = 200$, $L_y = 20$ and $L_z = 10.5$ has been chosen, x, y, and z being the streamwise, the wall-normal and the spanwise directions, respectively. After a grid-convergence analysis, a mesh made up by $901 \times 150 \times 61$ points – stretched in the wall-normal direction so that the height of the first cell close to the wall is equal to 0.1 – is selected. The nonlinear optimization has been performed for $Re_{in} = 610$ with initial energy $E_0 = 0.1$. The shape of the optimal perturbations shows large differences with respect to the linear case. Figure 1 provides the streamwise and spanwise component of the nonlinear optimal perturbation, at $t = 0$ and $t = T$, for the target time $T = 75$. In the first frame ($t = 0$) of Figure 1, one can observe the presence of two series of streamwise-alternated elongated patches of the spanwise component of the perturbation (blue and red surfaces), placed at the two flanks of a low-momentum flow region (green surfaces). Moreover, the regions where the streamwise component of the velocity disturbance is negative are associated with zones of positive wall-normal component. This means that the amplification of the perturbation is not only due to the lift-up effect, but is strongly affected by nonlinear interactions. In fact, at $t = T = 75$ (see the second frame of Figure 1), the classical streamwise-elongated streaks are not recovered, but one can observe the presence of a Λ-structure which strongly recalls the bulge in the streamwise fluctuation recently described in direct numerical simulations (DNS) of transition induced by travelling turbulence patches by Wu & Moin (2009). Such Λ-structures are here observed in the wall-normal and streamwise components of the velocity perturbation, whereas the spanwise component shows a sinuous shape along x. Similar shape and behaviour have been found for the optimal perturbation at higher target times for the same initial energy. Figure 2 shows the streamwise distribution of the spanwise-averaged skin-friction coefficient C_f at different times. The laminar and turbulent distributions of C_f are also reported for comparison. One can observe that, in the core of the propagating wave packet, for $T > 200$, C_f reaches values which are typical of turbulent flows. It is noteworthy that, at each time instant, a smooth-varying region is observed, recalling the *calm region* typical of the trailing edge of turbulent spots.

Figure 3 shows snapshots of the vortical structures identified by the Q-criterion and of the streamwise component of the perturbation extracted from the DNS at times $t = 0$, 35, 65, 95. The first frame shows the presence of alternated quasi-streamwise vortices, with an inclination in the (x, z) plane of about 4° with respect to the streamwise direction (in the linear case they are aligned with x). These vortices are tilted in the streamwise direction by the Orr mechanism, presenting at $t = 35$ (second frame) an inclination of about 10° in the (x, y) plane (not shown). Due to such an inclination, the downstream part of the vortex, which lies away from the wall, is convected downstream faster than the upstream part because it experiences higher base flow velocity; this causes the stretching and the amplification of such structures, which take the form of Λ-vortices. At the same time, such vortices induce patches of high- and low-velocity via the transport of the momentum associated with the base flow and with the finite amplitude streamwise perturbation. At $t = 65$ (third frame) the vortices are further stretched in the streamwise

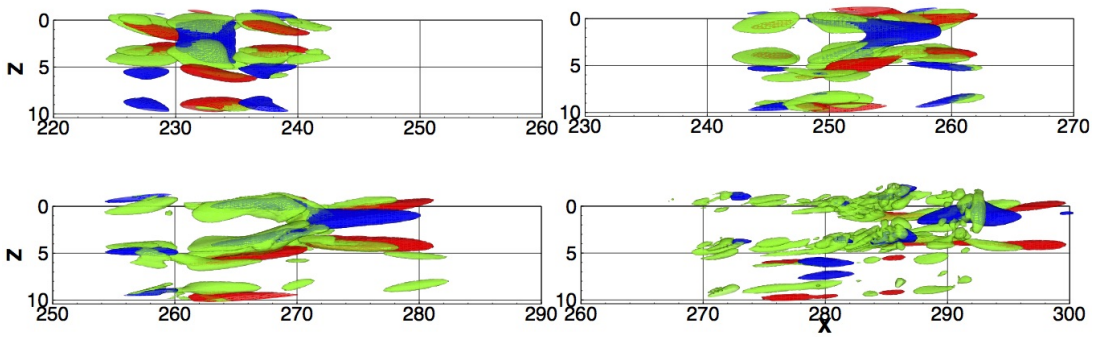

Figure 3: Snapshots of the perturbation at $t = 0$, 35, 65, 95, obtained by the DNS initialized by the nonlinear optimal for $T = 75$ and $E_0 = 0.01$. The green iso-surfaces refer to the Q-criterion; blue and red iso-surfaces refer to the negative and positive values of the streamwise velocity component, respectively.

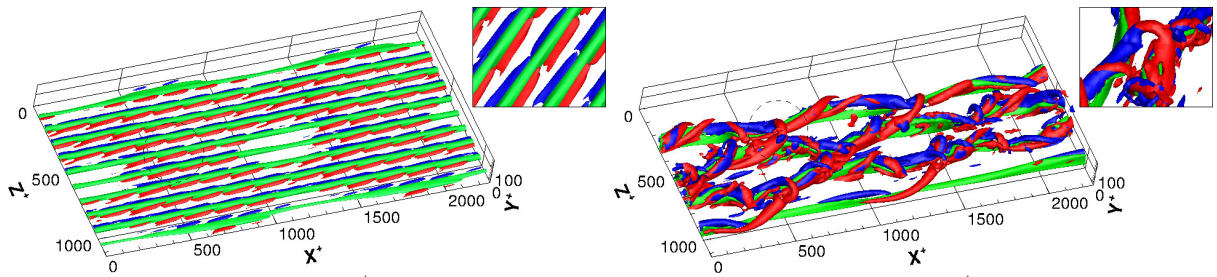

(a) $t^+ = T^+_{in}$ (b) $t^+ = T^+_{out}$

Figure 4: Optimal disturbance for T_{in} (left) and T_{out} (right) with $E_0 = 10^{-2}$. Isosurfaces of negative streamwise velocity (green) and Q-criterion colored by contours of streamwise vorticity (positive blue, negative red). The encircled regions are reported in a close-up on the right insets.

direction, so that a vortex filament oriented in the spanwise direction (the arch) is formed connecting the two quasi-streamwise vortices and inducing the formation of a hairpin, whose head is clearly visible at $t = 95$.

Turbulent flow

This section provides the analysis of turbulent channel flow at friction Reynolds number $Re_\tau = u_\tau h/\nu = 180$; u_τ, h, and ν being the friction velocity, the half-height of the channel, and the kinematic viscosity, respectively. The choice of studying a turbulent parallel flow is due to the need of reducing the computational cost of the simulations by using a more compact computational domain. Computations are performed using the spectral-element code NEK5000 (Fischer *et al.*, 2008), with Legendre polynomial reconstruction of degree 7 and second-order-accurate Runge-Kutta time integration scheme. Since two scaling of the variables are employed, variables expressed in inner units (normalized using u_τ and viscous length scale, $\delta_\nu = \nu/u_\tau$) are indicated with the superscript $^+$, whereas variables without any superscript are scaled in outer units (normalized using the centerline velocity U_c and h).
Incompressible flow is computed by solving the Navier–Stokes equations (NS) in a box having streamwise, wall-normal, and spanwise dimensions equal to $L_x = 4\pi$, $L_y = 2$, $L_z = 2\pi$,

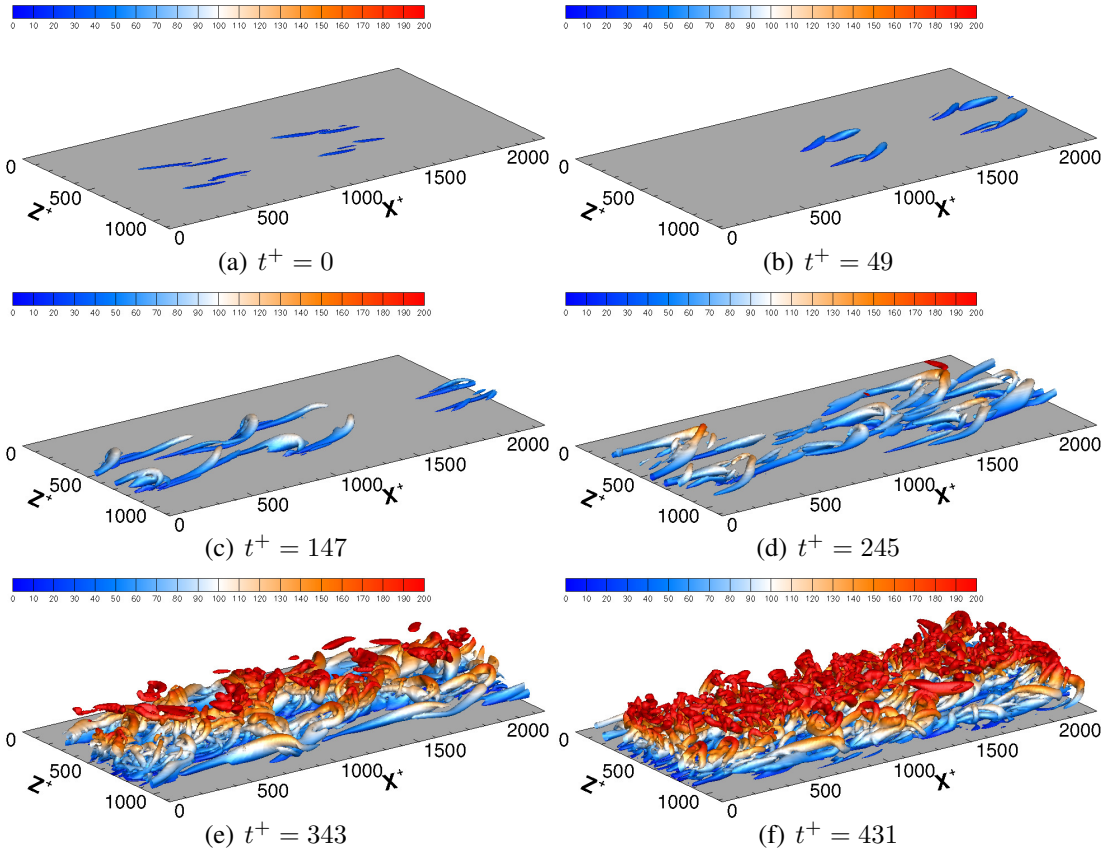

Figure 5: Snapshots of the time evolution of the outer optimal structures: isosurfaces of Q-criterion coloured by the wall normal distance y^+.

respectively. Dirichlet boundary conditions for the three velocity components are imposed at the walls, whereas periodicity is prescribed in the streamwise and spanwise directions.

A crucial independent parameter of the optimization procedure is the target time T, which is related to the lifetime of the coherent structures populating the flow. Butler & Farrell (1993) have chosen as representative of the time scale of coherent structures the eddy turnover time at $y^+ \approx 20$ (resulting in $T^+ = 80$ for $Re_\tau = 180$), finding optimal small-amplitude disturbances having the shape of low- and high-speed streaks with the inner typical spanwise spacing $\lambda_z^+ = 110$. Here, we employ the same criterion, choosing the inner optimization time $T_{in}^+ = 80$, ($T_{in} = 8.16$) roughly corresponding to one eddy turnover time evaluated in the buffer layer at $y^+ = 19$ (Butler & Farrell, 1993); and the outer optimization time $T_{out}^+ = 305$ ($T_{out} = 31.12$), corresponding approximately to one eddy turnover time at the centerline of the channel.

The resulting optimal finite-amplitude disturbance obtained for T_{in}^+ and $E_0 = 10^{-2}$ consists at $t = 0$ of alternated inclined streamwise vortices, flanking localized regions of streamwise velocity strong defects (not shown). Whereas, at T_{in}^+, the optimal disturbance consists of highly modulated streaks having a typical spanwise spacing of $\lambda_z^+ \approx 113$, surrounded by positive and negative streamwise vortices, with a spanwise spacing of about $\lambda_z^+ \approx 56$ (figure 4 (a)); this is a typical value recovered for vortex spacing in turbulent channel flow (Panton, 2001). Increasing the target time to the outer timescale T_{out}^+, the optimization algorithm provides a different flow structure. The initial optimal perturbation is strongly localized in space and is characterized by alternated streamwise vortices and localized patches of streamwise velocity perturbations

(not shown). At $t^+ = T^+_{out}$, this initial perturbation turns into a much more complex structure, mostly composed of packets of hairpin vortices on top of highly oscillating streamwise streaks, as shown in figure 4 (b). In particular, strong vortical structures are observed at two different scales. The small-scale structures are not symmetric and have spanwise length $\lambda_z^+ \approx 100$ (consistent with the observations of Zhou *et al.* (1999)). They are placed on top of the low-speed streaks, apparently as a result of their sinuous instability. On the other hand, the largest vortical structures have a clear symmetric hairpin shape, with typical wavelengths $\lambda_z \approx 2h$ and $\lambda_x \approx 2.5h$, consistent with the observations of turbulent bulges and packets of hairpin of length $\approx 2h$ (Adrian, 2007). To further characterize the dynamics of the outer nonlinear optimal perturbation, we analyze its time evolution. Figure 5 provides six snapshots of the optimal perturbation (Q-criterion isosurfaces, coloured by the wall-normal distance), from $t^+ = 0$ to $t^+ = 431$. The initial perturbation is localized in the three space directions and is composed of two packets of thin counter rotating vortices showing a spanwise symmetry, placed at $y^+ \approx 20$ (as indicated by the colours in figure 5 (a)). In figure 5 (b) one can observe the typical downstream tilting due to the Orr mechanism (Orr, 1907). Following the evolution of the perturbation, we can notice that the vortices tend to be lifted up from the wall towards the center of the channel, developing structures of increasing size in an inverse cascade from small to large scales (Jiménez, 1999). Concerning the vortical dynamics, one can observe the formation of new vortices aligned with the initial ones along modulated steamwise streaks (see figure 5 (c)). These vortices are lifted in the wall-normal direction, creating symmetric or non symmetric arches on top of the negative streaks at the wall, as one can observe in figure 5 (d). Once the small-scale hairpin and *cane* vortices have been created, some of them further grow and lift in the outer region (Adrian, 2007), as shown in figure 5 (e). When the structures have reached their maximum spatial growth, they begin to break-down, starting an energy cascade from the large scales towards the small ones, closing the loop towards the establishment of featureless turbulence (see figure 5 (f)).

CONCLUSIONS

Several experimental and numerical analysis have marked the importance of hairpin vortical structures in transitional and turbulent wall-bounded flows, indicating that such structures might represent a structural feature of wall-bounded turbulence. The present work aims at investigating whether the formation of hairpin structures in wall-bounded flow is governed by an energy maximization process on a suitable time scale. A nonlinear approach is employed for computing optimal perturbations, using a Lagrange-multipliers optimization technique coupled with a direct-adjoint iterative procedure.

For transitional flow, we have shown that optimal perturbations with large enough initial energies are localized in space and composed of spanwise-alternated thin vorticity tubes inclined with respect to the streamwise direction and placed around regions of large streamwise and wall-normal perturbations of opposite sign, resembling localized sweeps and ejections. Transition is triggered suddenly and occurs in a very localized region, inducing the formation of hairpin structures. Thus, hairpin vortex structures can be the outcome of a nonlinear optimal growth process, in a similar way as streaky structures are linked to a linear optimal growth mechanism.

For turbulent flows, different nonlinear optimal structures have been found. Depending on the chosen time scale for the energy growth they can have the shape of oscillating streaks or hairpin vortices. At least at moderate Reynolds numbers, we have found that also for turbu-

lent flows, nonlinear optimal structures at the outer scale correspond to hairpin vortices. The presence of optimal structures in turbulent flows confirms that the complex dynamics of such flows can be approximated by a low-dimensional dynamics. In fact, we have verified that such optimal coherent structures alone accurately approximate the characteristics of the entire turbulent flow since they well reproduce its spectrum, its velocity probability density function, its energy transfer mechanisms (Farano *et al.*, 2017). Reproducing these coherent structures from a superposition of simple modes, as proposed by Sharma & McKeon (2013) and Cohen *et al.* (2014) leads to the possibility of designing a reduced model of wall turbulence.

ACKNOWLEDGEMENTS

This work was granted access by HPC resources of IDRIS under allocation x20162a6362 made by GENCI. The authors also wish to acknowledge the computational resources of the PrInCE project (grant PONa3-00372-CUP D91D11000100007) at Politecnico di Bari.

References

ADRIAN, R J 2007 Hairpin vortex organization in wall turbulence. *Physics of Fluids* **19** (4), 041301.

BARKLEY, D, SONG, B, MUKUND, V, LEMOULT, G, AVILA, M & HOF, B 2015 The rise of fully turbulent flow . *Nature* **526**, 550–553.

BUTLER, K M & FARRELL, B F 1993 Optimal perturbations and streak spacing in wall-bounded turbulent shear flow. *Physics of Fluids A: Fluid Dynamics* **5** (3), 774–777.

CHERUBINI, S & DE PALMA, P 2013 Nonlinear optimal perturbations in a couette flow: bursting and transition. *Journal of Fluid Mechanics* **716**, 251–279.

CHERUBINI, S, DE PALMA, P & ROBINET, J-C 2015 Nonlinear optimals in the asymptotic suction boundary layer: Transition thresholds and symmetry breaking. *Physics of Fluids* **27** (3), 034108.

CHERUBINI, S, DE PALMA, P, ROBINET, J-C & BOTTARO, A 2010 Rapid path to transition via nonlinear localized optimal perturbations in a boundary-layer flow. *Physical Review E* **82** (6), 066302.

COHEN, J, KARP, M & MEHTA, V 2014 A minimal flow-elements model for the generation of packets of hairpin vortices in shear flows. *Journal of Fluid Mechanics* **747**, 30–43.

DUGUET, Y, MONOKROUSOS, A, BRANDT, L & HENNINGSON, D S 2013 Minimal transition thresholds in plane couette flow. *Physics of Fluids* **25** (8), 084103.

FARANO, M, CHERUBINI, S, ROBINET, J-C & DE PALMA, P 2016 Subcritical transition scenarios via linear and nonlinear localized optimal perturbations in plane poiseuille flow. *Fluid Dynamics Research* **48**, 061409.

FARANO, M, CHERUBINI, S, ROBINET, J.-C. & DE PALMA, P 2017 Optimal bursts in turbulent channel flow. *Journal of Fluid Mechanics* (in press, doi:10.1017/jfm.2017.107).

FISCHER, PF, LOTTES, JW & KERKEMEIR, SG 2008 nek5000 Web pages. http://nek5000.mcs.anl.gov.

FOURES, DPG, CAULFIELD, CP & SCHMID, PJ 2013 Localization of flow structures using ∞-norm optimization. *Journal of Fluid Mechanics* **729**, 672–701.

HALL, P & SMITH, F T 1991 On strongly nonlinear vortex/wave interactions in boundary-layer transition. *Journal of Fluid Mechanics* **227**, 641–666.

HAMILTON, J M, KIM, J & WALEFFE, F 1995 Regeneration mechanisms of near-wall turbulence structures. *Journal of Fluid Mechanics* **287**, 317–348.

JIMÉNEZ, J 1999 The physics of wall turbulence. *Physica A: Statistical Mechanics and its Applications* **263** (1), 252–262.

LEMOULT, G, SHI, L, AVILA, K, JALIKOP, S V, AVILA, M & HOF, B 2016 Directed percolation phase transition to sustained turbulence in Couette flow . *Nature Physics* **12**, 254–258.

NAGATA, M 1990 Three-dimensional finite-amplitude solutions in plane couette flow: bifurcation from infinity. *Journal of Fluid Mechanics* **217**, 519–527.

ORR, W M'F 1907 The stability or instability of the steady motions of a perfect liquid and of a viscous liquid. part ii: A viscous liquid. In *Proceedings of the Royal Irish Academy. Section A: Mathematical and Physical Sciences*, pp. 69–138. JSTOR.

PANTON, R L 2001 Overview of the self-sustaining mechanisms of wall turbulence. *Progress in Aerospace Sciences* **37** (4), 341–383.

PRINGLE, C CT, WILLIS, A P & KERSWELL, R R 2012 Minimal seeds for shear flow turbulence: using nonlinear transient growth to touch the edge of chaos. *Journal of Fluid Mechanics* **702**, 415–443.

SEYADI, T, CURTIS, W H & MOIN, P 2013 Direct numerical simulation of complete h-type and k-type transitions with implications for the dynamics of turbulent boundary layers. *Journal of Fluid Mechanics* **724**, 480–509.

SHARMA, A S & MCKEON, B J 2013 On coherent structures in wall turbulence. *Journal of Fluid Mechanics* **728**, 196–238.

TOMKINS, C D & ADRIAN, R J 2003 Spanwise structure and scale growth in turbulent boundary layers. *Journal of Fluid Mechanics* **490**, 37–74.

VERZICCO, R. & ORLANDI, P. 1996 A finite-difference scheme for three-dimensional incompressible flows in cylindrical coordinates. *J. Comput. Phys.* **123** (2), 402–414.

WALEFFE, F 1997 On a self-sustaining process in shear flows . *Physics of Fluids* **9**, 883–901.

WU, X & MOIN, P 2009 Forest of hairpins in a low-reynolds-number zero-pressure-gradient flat-plate boundary layer. *Physics of Fluids* **21** (9), 091106.

ZHOU, J, ADRIAN, R J, BALACHANDAR, S & KENDALL, TM 1999 Mechanisms for generating coherent packets of hairpin vortices in channel flow. *Journal of Fluid Mechanics* **387**, 353–396.